Journal Pre-proof

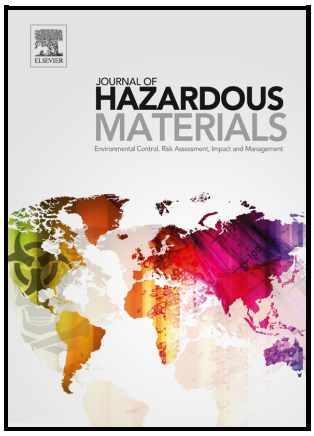

Polystyrene nanoplastics induce cardiotoxicity by upregulating HIPK2 and activating the P53 and TGF-β1/Smad3 pathways

Jian-Zheng Yang, Kai-Kai Zhang, Clare Hsu, Lin Miao, Li-Jian Chen, Jia-Li Liu, Jia-Hao Li, Xiu-Wen Li, Jia-Hao Zeng, Long Chen, Ji-Hui Li, Xiao-Li Xie, Qi Wang

PII: S0304-3894(24)01402-X

DOI: https://doi.org/10.1016/j.jhazmat.2024.134823

Reference: HAZMAT134823

To appear in: *Journal of Hazardous Materials*

Received date: 9 March 2024
Revised date: 16 May 2024
Accepted date: 3 June 2024

Please cite this article as: Jian-Zheng Yang, Kai-Kai Zhang, Clare Hsu, Lin Miao, Li-Jian Chen, Jia-Li Liu, Jia-Hao Li, Xiu-Wen Li, Jia-Hao Zeng, Long Chen, Ji-Hui Li, Xiao-Li Xie and Qi Wang, Polystyrene nanoplastics induce cardiotoxicity by upregulating HIPK2 and activating the P53 and TGF-β1/Smad3 pathways, *Journal of Hazardous Materials,* (2024) doi:https://doi.org/10.1016/j.jhazmat.2024.134823

Polystyrene nanoplastics induce cardiotoxicity by upregulating HIPK2 and activating the P53 and TGF-β1/Smad3 pathways

Jian-Zheng Yang[a,#], Kai-Kai Zhang[a,#], Clare Hsu[a], Lin Miao[b], Li-Jian Chen[a], Jia-Li Liu[a], Jia-Hao Li[a], Xiu-Wen Li[a], Jia-Hao Zeng[a], Long Chen[a], Ji-Hui Li[a], Xiao-Li Xie[c*], Qi Wang[a*]

[a] Guangzhou Key Laboratory of Forensic Multi-Omics for Precision Identification, School of Forensic Medicine, Southern Medical University, Guangzhou, Guangdong, 510515, China

[b] School of Forensic Medicine, Kunming Medical University, Kunming, China

[c] Department of Toxicology, School of Public Health, Southern Medical University (Guangdong Provincial Key Laboratory of Tropical Disease Research), Guangzhou, Guangdong, 510515, China

#**These authors contributed equally to this work and share first authorship.**

***Corresponding Authors:**

Xiao-Li Xie

E-mail: xiexiaoli1999@smu.edu.cn;

Qi Wang

E-mail: wangqi1980@smu.edu.cn

Abstract

Nanoplastics (NPs) pollution has become a global environmental problem, raising numerous health concerns. However, the cardiotoxicity of NPs exposure and the underlying mechanisms have been understudied to date. To address this issue, we comprehensively evaluated the cardiotoxicity of polystyrene nanoplastics (PS-NPs) in both healthy and pathological states. Briefly, mice were orally exposed to four different concentrations (0 mg/day, 0.1 mg/day, 0.5 mg/day, and 2.5 mg/day) of 100-nm PS-NPs for 6 weeks to assess their cardiotoxicity in a healthy state. Considering that individuals

with underlying health conditions are more vulnerable to the adverse effects of pollution, we further investigated the cardiotoxic effects of PS-NPs on pathological states induced by isoprenaline. Results showed that PS-NPs induced cardiomyocyte apoptosis, cardiac fibrosis, and myocardial dysfunction in healthy mice and exacerbated cardiac remodeling in pathological states. RNA sequencing revealed that PS-NPs significantly upregulated homeodomain interacting protein kinase 2 (HIPK2) in the heart and activated the P53 and TGF-beta signaling pathways. Pharmacological inhibition of HIPK2 reduced P53 phosphorylation and inhibited the activation of the TGF-β1/Smad3 pathway, which in turn decreased PS-NPs-induced cardiotoxicity. This study elucidated the potential mechanisms underlying PS-NPs-induced cardiotoxicity and underscored the importance of evaluating nanoplastics safety, particularly for individuals with pre-existing heart conditions.

Keywords:

Polystyrene nanoplastics, cardiotoxicity, homeodomain interacting protein kinase 2, TGF-β1/Smad3 signaling pathway, P53 signaling pathway

1. Introduction

Plastic products, while offering convenience, also contribute to serious pollution issues (Deweerdt, 2022). These plastics degrade into micro- and nanoplastics (MNPs), which are widespread in both the environment and the human body (Amato-Lourenço et al., 2021; Luo et al., 2022; Ragusa et al., 2021). The average human ingestion of plastic particles is estimated to be 0.23-11.9 mg/kg per day, with oral exposure being the main route of intake (Prata et al., 2020; Senathirajah et al., 2021). This exposure is concerning, given the potential toxic effects associated with plastic ingestion. A recent study underscored the continuous fragmentation of microplastics into nanoplastics (NPs), suggesting a substantial increase in their quantities (WagnerReemtsma, 2019). The smaller size of NPs enhanced their ability to penetrate biological barriers, and evidence of the potential for NPs to cross these barriers further exacerbated these apprehensions about their impact on human health and the environment (Fournier et al.,

2020; Liang et al., 2021; Sun et al., 2020).

Recent advancements in understanding NPs toxicity have revealed that NPs exposure could lead to significant damages to the liver, intestine, lung, and vascular system, as well as to neurotoxicity and reproductive toxicity (Li et al., 2023; Liang et al., 2022; Ma et al., 2023; Wang et al., 2023; Wang et al., 2023; Zha et al., 2023). Despite evidence of NPs accumulation in the heart, research on their cardiotoxicity remains scarce (Liang et al., 2021; Lin et al., 2022).

It is imperative to recognize that individuals with pre-existing health conditions are not only inevitably exposed to environmental pollutants but also disproportionately susceptible to its adverse effects (Manzano-Covarrubias et al., 2023). Many of these pollutants are established risk factors for a range of diseases, particularly cardiovascular diseases (Wu et al., 2023). The heightened vulnerability of individuals with pre-existing health conditions to environmental pollutants, particularly NPs, underscores the necessity for more focused studies on the impacts of NPs on cardiac health in pathological states. With limited data in this area, there is a clear need for a deeper understanding of how NPs affect the heart, particularly in those already facing health challenges.

HIPK2 belongs to the family of serine/threonine protein kinases (HIPK1, HIPK2, HIPK3, and HIPK4) and has been implicated in various biological processes, including signaling, cell proliferation, and apoptosis (ContePierantoni, 2018; Kim et al., 1998; RitterSchmitz, 2019). The phosphorylation of P53 is a major mechanism mediating myocardial apoptosis (Kim et al., 2013), while the TGF-β1/Smad3 pathway is a classical signaling cascade involved in the progression of cardiac fibrosis (Weng et al., 2023). Current research suggests that HIPK2 could be an upstream regulator of both P53 and the TGF-β/Smad3 pathways (Jin et al., 2012). Given the potential role of HIPK2 in regulating these key pathways, we investigated its involvement in the context of PS-NPs-induced cardiotoxicity.

In this study, we focused on PS-NPs, one of the most common NPs in the environment (Rai et al., 2021). Healthy mice were subjected to continuous exposure to PS-NPs for six weeks to assess their cardiotoxic effects. Additionally, to investigate the

cardiotoxic effects of PS-NPs in pathological states, we employed a model using isoprenaline-induced cardiac remodeling. We utilized RNA sequencing and pharmacological inhibition assays to specifically investigate the genetic and molecular pathways involved. Our focus was on the key gene *Hipk2* and its role in activating crucial signaling pathways, notably the P53 and TGF-beta pathways. This study enhanced our understanding of the cardiotoxicity associated with oral PS-NPs exposure in both healthy and pathological states.

2. Methods and Materials

2.1. Chemicals

The 100-nm diameter polystyrene nanoplastics (PS-NPs) were purchased from Tesulang Chemical Materials Co., Ltd. (Cat #: 65568898989, Purity > 99%, Dongguan, China) and were suspended in sterile Milli-Q water. The morphology and size of the PS-NPs were characterized by a scanning electron microscope (TESCAN VEGA3 SEM, Brno, Czech) and a particle size analyzer (Zetasizer NANOZS, Malvern, UK) (Figure S1A-B). Isoprenaline hydrochloride (ISO) (Cat #: I5627, Sigma–Aldrich, St. Louis, MO, USA; CAS #: 51-30-9) was dissolved in a sterile saline solution. Protein kinase inhibitor 1 hydrochloride (PKI1H) (Cat #: HY-U00439A, MedChemExpress, Monmouth Junction, NJ, U.S.A., CAS #: 2321337-71-5) was dissolved in sterile Milli-Q water.

2.2. Animals and ethical approval

C57BL/6 male mice (6 weeks, 18-20 g, SPF grade) were purchased from the Southern Medical University Animal Center and kept under special pathogen-free (SPF) environmental conditions during the entire experimental period (23 ± 2°C, 12 h light/dark cycle). We followed the animal ethics committee guidelines, and the Laboratory Animal Ethics Committee of Southern Medical University (Ethical Approval Code: L2023102) approved all the animal experiments.

2.3. Experimental design

Based on previous studies of plastic intake doses in humans and exposure dose conversion equations between mice and humans, the equivalent dose was approximately 0.05-2.9 mg/day for a 0.02 kg mouse. Therefore, we selected doses of 0.1, 0.5, and 2.5 mg/day to comprehensively evaluate the cardiotoxic effects of PS-NPs across a spectrum of exposures (NairJacob, 2016; Xu et al., 2023).

Experiment I: After one week of adaptive feeding, to investigate the cardiotoxicity in healthy mice at different environment-related concentrations, we randomly divided the mice into four groups (n = 8 per group): the control group (Con), fed with 0.2 ml of sterile Milli-Q water. PS-NPs groups (L-NPs, M-NPs, or H-NPs) at doses of 0.1, 0.5, or 2.5 mg/d, orally administered with 0.2 ml of PS-NPs suspensions at concentrations of 0.5, 2.5, or 12.5 mg/ml. To establish the treatment duration, we referenced several studies that demonstrated significant organ-specific toxicities following 6 weeks of PS-NPs exposure. These include severe neurotoxicity (Kang et al., 2023), hematopoietic toxicity (Jing et al., 2022), nephrotoxicity (Tang et al., 2023), hepatotoxicity and enterotoxicity (Huang et al., 2023). Therefore, we treated all the mice for 6 consecutive weeks to adequately explore the cardiotoxic effects of PS-NPs. This duration is depicted in the schematic illustration of the experimental flow (Figure 1A).

Experiment II: Considering that individuals with underlying health conditions are more susceptible to the adverse effects of environmental pollutants, we further investigated the cardiotoxic effects of PS-NPs on pathological states. In this part of the study, we used moderate doses of PS-NPs to exacerbate ISO-induced cardiac remodeling (n = 8 per group), as illustrated in Figure 4A. Specifically, M-NPs suspension (0.5mg/d) was treated orally once daily for 6 weeks, and ISO (5 mg/kg/d) was injected subcutaneously starting in the fifth week. The selected dose of ISO has been previously demonstrated to induce cardiac remodeling in mice, making it a standard model for studying the effects of drugs or other interventions on the progression of cardiac pathology (Wang et al., 2020). The control mice received an equal volume of Milli-Q water or saline in the same manner.

Experiment III: To explore the role of HIPK2 in PS-NPs-mediated cardiotoxicity, we divided the mice into six groups (n = 8 per group): Control group, PKI1H group, H-

NPs group, PKI1H+H-NPs group, ISO+M-NPs group, and PKI1H +ISO+M-NPs group. The treatment of ISO and different doses of PS-NPs were consistent with the above. Previous studies have demonstrated that PKI1H effectively suppresses HIPK2 expression and does not exhibit cardiotoxic effects when administered continuously throughout the study period (Zhou et al., 2021; Zhou et al., 2022). Based on the dosages used in these studies, we administered PKI1H to mice at a dosage of 200 μg/kg/day via oral gavage. This treatment was initiated two hours prior to the introduction of PS-NPs to ensure adequate systemic absorption and was maintained daily for a period of 6 consecutive weeks (Figure 7A).

2.4. Transthoracic echocardiography (TTE)

Vevo 2100 echocardiography system (FUJIFILM Visualsonics, Toronto, ON, Canada) was used to evaluate the cardiac structure and function of the mice in each batch. Before TTE, the mice were anesthetized with 1% isoflurane (RWD, Life Science Co., Ltd., China), and their chest hair was removed. Left ventricular systolic function was assessed through M-mode echocardiography. Images were obtained from the left parasternal short axis, and measurements were taken from three consecutive cardiac cycles. As previously described, various parameters of the left ventricle (LV) were recorded in the present study, in which the LV ejection fraction (EF) and fractional shortening (FS) were calculated (Wang et al., 2020).

2.5. Tissue collection

After TTE, all animals were anesthetized with 50 mg/kg pentobarbital (Zhang et al., 2023). Mouse serum samples were obtained by centrifugation (4000 g, 10 min, 4°C) after standing at room temperature for 30 min. Heart tissues were collected and stored at -80°C, and a portion of the heart tissue was fixed in 4% paraformaldehyde for further analysis.

2.6. Histological assessment

2.6.1. H&E and Masson staining

The heart tissues were fixed with 4% paraformaldehyde for 48 h and embedded in paraffin wax. The tissues were then cut into 5-μm sections. Hematoxylin and eosin (H&E) staining and Masson's trichrome staining (Cat #: G1346, Solarbio) were used to evaluate general myocardium morphology and cardiac fibrosis. For quantification of Masson staining, five fields of view were selected for each section, and their mean values were obtained. Four sections were chosen for each group, and the values were calculated.

2.6.2. TUNEL staining

For TUNEL staining, we used the Roche In Situ Cell Death Detection Kit (Cat #: 11684817910) to detect apoptosis in cardiac tissue. Briefly, paraffin sections were routinely deparaffinized, hydrated, and permeabilized. Next, 10% goat serum was used for closure, the TUNEL reaction mixture (50 μl) was added dropwise, and TBS was added dropwise as a negative control. Finally, the positive cells were stained using diaminobenzidine (DAB). The apoptotic rate was defined as the proportion of brown apoptotic cardiomyocyte nuclei to total cardiomyocyte nuclei in the same field of view, ten fields of view were quantified to determine the mean value for each section, and four sections were utilized for each group.

2.6.3. Immunohistochemistry (IHC)

Paraffin-embedded heart sections were deparaffinized, hydrated, antigenically repaired, and blocked with 10% goat serum. Each tissue sample was titrated with 100 μl of primary antibody working solution and incubated overnight at 4°C. The next day, after fifteen minutes of rewarming at room temperature, the sections were washed and incubated with secondary antibody for 45 min at 37°C. Finally, the color was developed using freshly prepared DAB. Rabbit anti-HIPK2 (Proteintech, Cat #: 55408-1-AP, dilution ratio: 1:300) was used as the primary antibody in this study, and the corresponding goat anti-rabbit HRP (Abcam, Cat #: ab205718, dilution ratio: 1:2000) was used as the secondary antibody. The nuclei of HIPK2-positive cells were stained brownish yellow.

All images of the stained slides were captured with a light microscope (KF-PRO-005-EX, China), and ImageJ (version 1.52i) was utilized to assess the collagen content and apoptotic rate.

2.7. Biochemical analysis

Serum samples were used to assess relevant indicators of myocardial injury. According to the manufacturer's instructions (Jiangsu Meimian Industrial Co., Ltd.), the following ELISA kits were used: cTnT (Cat #: MM-0945M1), CK-MB (Cat #: MM-43703M1), AST (Cat #: MM-44384M1), and α-HBDH (Cat #: MM-0604M1). The OD value of each sample was measured at 450 nm using a microplate reader (Thermo Scientific, Waltham, MA, USA), and the concentration of each index was calculated according to the standard curve (Yang et al., 2023).

2.8. Western blotting (WB)

Total protein lysates from left ventricular tissues were extracted with RIPA buffer (Beyotime, Shanghai, China) containing 1% PMSF and 1% phosphatase inhibitor, and the total protein concentration was determined with a BCA protein quantification kit (Thermo Scientific). Next, equal amounts of proteins were separated using 12% SDS–PAGE and transferred to a PVDF membrane (Millipore) with a pore size of 0.22 μm, as described previously (Zhang et al., 2022). The membranes were blocked with 5% nonfat milk for 2 h and then incubated with primary antibodies overnight at 4°C before they were incubated with secondary antibodies for 1 h at room temperature. The primary antibodies used included HIPK2 (Proteintech, Cat #: 55408-1-AP, dilution ratio: 1:1000), phospho-P53 (Ser15) (Cell Signaling Technology, Cat #: 9284S, dilution ratio: 1:1000), P53 (Proteintech, Cat #: 21891-1-AP, dilution ratio: 1:1000), Caspase3 (ABclonal, Cat #: A2156, dilution ratio: 1:800), GAPDH (Proteintech, Cat #: 60004-1-Ig, dilution ratio: 1:2000), TGF-β1 (Abcam, Cat #: ab215715, dilution ratio: 1:1000), phospho-Smad3 (ABclonal, Cat #: AP0727, dilution ratio: 1:1000), Smad3 (ABclonal, Cat #: A19115, dilution ratio: 1:1000), and Col1a1 (ABclonal, Cat #: A1352, dilution ratio: 1:1000).

2.9. Reverse transcription quantitative polymerase chain reaction (RT–qPCR)

As described previously (Yang et al., 2023), we completed the extraction and concentration determination of total RNA from the left ventricle. Next, RNA samples (1 μg from each sample) were reverse transcribed into cDNA using the StarScript III All-in-one RT Mix with gDNA Remover (Cat. #: A230-10, GenStar, China). Finally, cDNA samples were amplified on a Roche LightCycler 480 using a 2× RealStar Green Fast Mixture (A301-10, GenStar). The $2^{-\Delta\Delta Ct}$ method was used to analyze the data. Sequence information for the primers was included in the Table S1.

2.10. RNA sequencing analysis

Total RNA was extracted from the left ventricle using a TRIzol reagent. The quality and quantity of the RNA samples were determined using a NanoDrop 2000 spectrophotometer (Zhang et al., 2023). Next, the RNA-Seq transcriptome library was constructed using an Illumina TruSeq library construction kit following the manufacturer's instructions. Subsequently, Majorbio Bio-Pharm Technology Co., Ltd. (Shanghai, China) sequenced the library on an Illumina HiSeq 4000 platform. The paired-end reads were subjected to trimming and quality control using fastp with default parameters (https://github.com/OpenGene/fastp). Subsequently, the clean reads were individually aligned to the reference genome using HISAT2 software in orientation mode (http://ccbjhu.edu/software/hisat2/index.shtm1). The mapped reads from each sample were assembled using StringTie via a reference-based approach. Differentially expressed genes (DEGs) were identified by applying the criteria of a fold change (FC) ≥ 2 or ≤ 0.5 and a p value ≤ 0.05. The following analytical techniques were employed on the Majorbio I-Sanger Cloud Platform (https://cloud.majorbio.com) for the present analysis: principal component analysis (PCA), volcano plot, Venn diagram, and Kyoto Encyclopedia of Genes and Genomes (KEGG) enrichment analysis.

2.11. Statistical analysis

The data were reported as the mean ± standard error of the mean (SEM). Statistical

analysis was performed using IBM SPSS Statistics (version 26.0). The Shapiro–Wilk normality test was used to assess the data distribution. For normally distributed data, significant differences were determined using one-way ANOVA followed by Tukey's multiple comparisons test or two-way ANOVA followed by Tukey's multiple comparisons test. For nonnormally distributed data, the Kruskal-Wallis test was used, followed by Dunn's post hoc test. A p value less than 0.05 was considered to indicate statistical significance. For RNA sequencing analysis, PCA was conducted using the eigenvalue of the covariance matrix method, and differential analysis of DEGs was performed based on DESeq2.

3. Results

3.1. Dose-dependent cardiotoxicity of PS-NPs in healthy mice

To assess the cardiotoxic effects of environmentally relevant concentrations of PS-NPs, healthy mice were continuously exposed to low (L-NPs), medium (M-NPs), or high (H-NPs) doses of PS-NPs by oral administration for six weeks (Figure 1A). A scanning electron microscope and particle size analyzer were utilized to measure the shape and diameter of the PS-NPs. As shown in Figure S1A-B, the PS-NPs used in this study were round NPs with an average particle size of 84.32 nm. There were no significant changes in the food intake, water intake, and body weight of the mice in each group during the whole experiment (Figure S1C). We performed a TTE assay, which showed no significant difference in heart rate among the four groups (Figure 1B), while mice in the H-NPs group exhibited the lower EF and FS compared with those in the control group, indicating the occurrence of myocardial systolic dysfunction (Figure 1C). Serum biochemical analysis revealed that the biomarkers used for diagnosing myocardial injury, cTnT, CK-MB, AST, and α-HBDH, were significantly elevated in the M-NPs and H-NPs groups (Figure 1D). Histologically, H&E staining was used to assess the general condition of the heart and showed that M-NPs promoted inflammatory cell infiltration, while H-NPs promoted concomitant interstitial fibrosis (Figure 1E). However, PS-NPs did not cause cardiac hypertrophy, as demonstrated by the absence of differences in the heart weight/body weight (HW/BW) ratio and HW/tibia length

(HW/TL) among the four groups (Figure 1F). Masson staining and RT–qPCR demonstrated that compared with Con, H-NPs induced an increase in the collagen content (Figure 1G-H), with a corresponding increase in the mRNA levels of fibrosis-associated genes (Figure 1K), including *Col1a1* (collagen, type I, alpha 1) and *Col3a1* (collagen, type III, alpha 1). TUNEL staining and RT–qPCR demonstrated that both M-NPs and H-NPs led to increased apoptosis in cardiomyocytes (Figure 1I-J) and upregulated the proapoptotic gene *Bax*, but the mRNA level of the antiapoptotic gene *Bcl-2* was unchanged (Figure 1L). These results suggested that PS-NPs cause apoptosis, fibrosis, and systolic dysfunction in the mouse heart in a dose-dependent manner under physiological conditions.

3.2. Transcriptome analysis of mouse hearts exposed to different doses of PS-NPs

To elucidate the potential mechanism of PS-NPs-induced cardiotoxicity, we performed RNA sequencing analysis. PCA showed that the Con group and the remaining three groups were clustered separately, with the M-NPs and H-NPs groups being more similar in composition (Figure 2A). No significant myocardial damages was observed after 6 weeks of oral exposure to L-NPs, and we focused on the transcriptomic changes in the M-NPs and H-NPs groups. The number of DEGs increased gradually with increasing exposure dose (Figure 2B). Specifically, 233 genes were upregulated and 167 genes were downregulated in the M-NPs group. H-NPs resulted in 284 upregulated genes and 274 downregulated genes. The volcano plot also showed the top 6 most significant genes filtered based on the p value, five of which were present in both M-NPs and H-NPs (Figure 2C). The heatmap further depicted the mRNA levels, showing the most pronounced and dose-dependent increase in *Hipk2* expression compared to that in the Con group. The log2FC values for *Pdpr*, *Ubxn2a*, and *Hipk2* were 1.22, 1.90, and 2.06, respectively (Figure 2D). A Venn diagram showed that there were 400 M-NPs-regulated DEGs, 558 H-NPs-regulated DEGs, and 189 co-regulated DEGs (Figure 2E). We performed KEGG enrichment analysis on the crossed 189 DEGs and identified the top 20 enriched pathways, among which the apoptosis-related P53 pathway was significantly enriched (Figure 2F). Given that M-NPs and H-NPs caused different

degrees of cardiotoxicity, we next analyzed the genes regulated by each of them in parallel. The enrichment results showed that they were co-enriched to the P53 signaling pathway, which plays a crucial role in regulating apoptosis, whereas H-NPs-regulated DEGs were additionally enriched in the ECM-receptor interaction and TGF-beta signaling pathway, which were closely associated with cardiac fibrosis (Figure 2G). These results suggested that PS-NPs significantly upregulated *Hipk2* in the heart and activated the P53 and TGF-beta signaling pathways, which might be potential mechanisms underlying the cardiotoxicity induced by PS-NPs exposure.

3.3. Increased phosphorylation of P53 and activation of the TGF-β1/Smad3 pathway mediate PS-NPs-induced cardiotoxicity

Based on the results of mRNA sequencing analysis, we validated the upregulation of HIPK2 in the M-NPs and H-NPs groups compared to that in the Con group by IHC and WB analysis (Figure 3A-B). Phosphorylation of P53 (P-P53) at serine 15 has been implicated in cardiomyocyte apoptosis (Kim et al., 2013), and previous studies have demonstrated that the TGF-β1/Smad3 signaling pathway played a key role in cardiac fibrosis under various pathological conditions (BujakFrangogiannis, 2007; Lin et al., 2019). Guided by these KEGG enrichment results and the well-established roles of these pathways in cardiac pathology, we selected the P53 and TGF-β1/Smad3 pathways for further validation, and WB analysis revealed that M-NPs and H-NPs increased the phosphorylation of P53 and the cleaved Caspase3/Caspase3 ratio at the protein level, suggesting that increased phosphorylation of P53 mediates PS-NPs-induced apoptosis in the heart (Figure 3C). Consistent with the sequencing data, the results of WB analysis showed that H-NPs activated the TGF-β1/Smad3 pathway and caused an increase in the Col1a1 protein level by upregulating TGF-β1 and the phosphorylation of Smad3, suggesting that H-NPs mediated the cardiac fibrosis caused by PS-NPs (Figure 3D). The above results suggested that PS-NPs could stimulate apoptosis and fibrosis in healthy hearts through increased phosphorylation of P53 and activation of the TGF-β1/Smad3 pathway.

3.4. Effects of PS-NPs exposure on the hearts of mice in pathological states

Environmental pollutants are known to exacerbate the progression of heart failure in patients with pre-existing cardiac conditions (RajagopalanLandrigan, 2021). To comprehensively evaluate the cardiotoxic effects of PS-NPs, our study extended the scope to include their impact on the heart under pathological conditions. ISO, a β-adrenergic agonist, is known to induce cardiac fibrosis and hypertrophy, which are pivotal factors in the development of cardiac insufficiency and heart failure (Yang et al., 2023; Zhang et al., 2022). Considering the realistic exposure levels of NPs in environmental contexts and our preliminary findings that M-NPs alone can induce significant myocardial apoptosis and cardiac enzyme elevation without causing overt dysfunction, we designed Experiment II to assess the impact of M-NPs in conjunction with ISO on the progression of cardiac disease. This model aimed to simulate combined stressors that might be encountered in at-risk human populations. The schematic representation of this experimental model was depicted in Figure 4A. The TTE results showed that mice in the ISO+M-NPs group exhibited the lower EF and FS than mice in the Con group, suggesting that combined exposure resulted in myocardial systolic dysfunction (Figure 4B-C). Biochemical analyses revealed that ISO induced elevated markers of myocardial injury, and M-NPs further exacerbated these changes (Figure 4D). H&E staining (Figure 4E) and Masson staining showed that ISO induced cardiac fibrosis, and elevated HW/BW and HW/TL indicated that ISO induced cardiac hypertrophy, which suggested that ISO-induced cardiac remodeling. However, M-NPs did not exacerbate ISO-induced cardiac hypertrophy (Figure 4F) but exacerbated collagen fiber deposition (Figure 4G-H). TUNEL staining revealed that compared with ISO treatment alone, combined exposure to ISO+M-NPs resulted in a greater rate of apoptosis (Figure 4I-J). We assessed the mRNA levels of fibrosis and apoptosis indicators using RT–qPCR and showed that ISO+M-NPs caused a further increase in the mRNA levels of *Co1a1*, *Col3a1*, and *Bax* compared to the ISO group, while the mRNA level of the antiapoptotic gene *Bcl-2* was not significantly altered (Figure 4K–L). The results in this section suggested that M-NPs exacerbated ISO-induced cardiac remodeling, mainly in terms of apoptosis and fibrosis.

3.5. Transcriptome analysis of mouse hearts exposed to PS-NPs in pathological states

We used RNA-seq analysis to explore the potential mechanisms by which M-NPs exacerbated the pathological state of the heart. The PCA results showed that the ISO and ISO+M-NPs groups were clustered separately (Figure 5A). A volcano plot revealed 1515 DEGs between the ISO+M-NPs and ISO groups, of which 751 were upregulated and 764 were downregulated in the ISO+M-NPs group. Interestingly, among the top 6 DEGs most significantly altered according to the p value, *Hipk2* was also significantly upregulated in the ISO+M-NPs group (Figure 5B). KEGG enrichment analysis of 1515 DEGs revealed that the fibrosis-associated "ECM-receptor interaction" and "TGF-beta signaling pathway", as well as the apoptosis-associated "P53 signaling pathway", were similarly enriched (Figure 5C). A heatmap of the genes enriched in fibrosis-related pathways revealed the upregulation of type I, IV, VI, and IX collagen genes in the ISO+M-NPs group compared to the ISO group (Figure 5D). Taken together, in the state of cardiac remodeling, M-NPs also significantly upregulated *Hipk2* and activated the P53 and TGF-beta pathways.

3.6. PS-NPs further increased the phosphorylation of P53 and activated the TGF-β1/Smad3 pathway to exacerbate ISO-induced cardiac apoptosis and fibrosis

To validate the RNA sequencing results, we used IHC and WB analyses to confirm the upregulation of HIPK2 in the ISO+M-NPs group compared to the ISO group (Figure 6A-B). At the protein level, ISO increased the ratios of P-P53/P53 and cleaved Caspase3/Caspase3, and ISO+M-NPs exacerbated these changes (Figure 6C). Compared with ISO, ISO+M-NPs further elevated the expression of TGF-β1, the P-Smad3/Smad3 ratio, and the level of Col1a1 (Figure 6D). The above results suggested that PS-NPs further increased the phosphorylation of P53 and the activation of the TGF-β1/Smad3 pathway under ISO-induced pathological conditions.

3.7. HIPK2 inhibition protected against PS-NPs-induced cardiotoxicity

We noticed that in the present study, cardiac contractile dysfunction was induced in H-NPs- and ISO+M-NPs-treated mice, and the key gene *Hipk2* was consistently upregulated. To further investigate the role of HIPK2 in PS-NPs-induced cardiotoxicity, we pharmacologically inhibited HIPK2 using PKI1H both in the H-NPs and ISO+M-NPs groups. The experimental design was shown in Figure 7A. Mice in the H-NPs group treated with a HIPK2 inhibitor (PKI1H) exhibited preserved cardiac function, as confirmed by increased EF and FS (Figure 7B-C). Notably, PKI1H had no significant influence on the control mice (Figure 7). H-NPs treatment caused the release of cTnT, CK-MB, AST and α-HBDH into the bloodstream, and these effects were ameliorated by PKI1H. Morphologically, the H-NPs-induced increases in collagen fiber accumulation (Figure 7E, G-H) and myocardial apoptosis (Figure 7I-J) were reversed by PKI1H treatment. HW/BW and HW/TL did not differ between the H-NPs and PKI1H+H-NPs groups. At the mRNA level, PKI1H treatment inhibited the H-NPs-induced upregulation of *Col1a1*, *Col3a1,* and *Bax* (Figure 7K-L). Previous studies have shown that HIPK2 inhibition reduced P-P53 expression to attenuate myocardial apoptosis and protect against myocardial infarction (Zhou et al., 2021), and the TGF-β1/Smad3 pathway was a target of HIPK2 in multiorgan fibrosis (He et al., 2017; Liu et al., 2017). In the present study, WB analysis revealed that compared with Con, H-NPs increased the P-P53/P53 ratio and cleaved Caspase3/Caspase3 ratio, and these changes were reversed by PKI1H treatment (Figure 7M). On the other hand, H-NPs elevated the expression of TGF-β1, P-Smad3/Smad3, and Col1a1, which was ameliorated by PKI1H (Figure 7N). The above results suggested that inhibition of HIPK2 attenuated H-NPs-mediated cardiotoxicity by decreasing P53 phosphorylation and inhibiting the TGF-β1/Smad3 pathway.

We next investigated the role of HIPK2 inhibition in ISO+M-NPs-induced cardiotoxicity. Compared with ISO+M-NPs group, PKI1H treatment ameliorated cardiotoxicity, as evidenced by increased EF and FS (Figure 8A-B), decreased release of myocardial injury markers (Figure 8C), and decreased levels of fibrosis and apoptosis (Figure 8D, F-I). Notably, PKI1H also attenuated ISO+M-NPs-induced cardiac hypertrophy, as confirmed by decreased HW/BW and HW/TL (Figure 8E). At

the mRNA level, the ISO+M-NPs-induced upregulation of *Col1a1*, *Col3a1,* and *Bax* was reversed by PKI1H (Figure 8J-K). Similarly, compared with ISO+M-NPs treatment, PKI1H treatment reduced the P-P53/P53 ratio, cleaved Caspase3/Caspase3 ratio, P-Smad3/Smad3 ratio, and protein expression levels of TGF-β1 and Col1a1 (Figure 8L-M). These results suggested that HIPK2 inhibition also suppressed ISO+M-NPs-induced cardiotoxicity by attenuating P53 phosphorylation and inhibiting the TGF-β1/Smad3 pathway.

Briefly, in this section, we identified the important role of HIPK2 in PS-NPs-induced cardiotoxicity, whereas altered P53 phosphorylation and the TGF-β1/Smad3 pathway might be the underlying mechanism.

4. Discussion

Most studies on MNPs-mediated cardiotoxicity have focused on MPs (Zhang et al., 2022; Zhou et al., 2023). Compared to larger plastic particles, NPs may exhibit increased toxicity due to their smaller size and ability to penetrate biological barriers. Despite their potential toxicity, NPs have received less research attention, and the toxicologic mechanisms underlying their cardiac effects remain poorly understood. In the present study, we orally administered PS-NPs to mice at four different environmentally relevant concentrations to assess their impact on cardiac health in a healthy state. Recognizing that individuals with pre-existing cardiac conditions were generally more susceptible to environmental pollutants (Lim, 2021), we extended our investigation to explore the cardiotoxic effects of PS-NPs in pathological states. This was achieved by inducing cardiac pathologies in mice using ISO, a compound known to cause apoptosis, fibrosis, and hypertrophy in the heart. These conditions broadly represented major aspects of human cardiac diseases, making them an ideal model for our study (Guo et al., 2023; Wang et al., 2022). Our study provided valuable insights into the potential cardiac health effects of environmentally relevant concentrations of PS-NPs. Our findings contributed to the growing body of evidence needed for a comprehensive assessment of the risks posed by plastics to human health and the environment. Furthermore, our work provided a scientific foundation for future

research directions in this critical area.

Our study demonstrated that 6 weeks of oral exposure to M-NPs or H-NPs in healthy mice led to elevated markers of myocardial injury and increased cardiac apoptosis. Specifically, H-NPs were also found to induce cardiac fibrosis and systolic dysfunction, as evidenced by the H&E, Masson, and TTE results. This increased fibrosis resulted in decreased cardiac compliance, thereby accelerating heart failure progression (Ishiura et al., 2022). Given that environmental fine particulate matter is a known risk factor for cardiovascular disease progression and that individuals with pre-existing heart conditions are more susceptible to environmental pollutants (BrunekreefHoffmann, 2016; Wang et al., 2021), assessing the cardiotoxic effects of NPs in pathological states is highly important. Our findings revealed that in such pathological states, M-NPs notably exacerbated cardiac apoptosis and fibrosis without notably affecting cardiac hypertrophy, ultimately impairing cardiac systolic function. Furthermore, RNA sequencing indicated that PS-NPs upregulated *Hipk2* in the hearts of both healthy and pathological mice, underscoring the pivotal role of HIPK2 in PS-NPs-induced cardiotoxicity.

Earlier studies have indicated that HIPK2 was critical for maintaining basal cardiac function (Guo et al., 2019) and was observed unregulated in myocardial infarction (Zhou et al., 2021), heart failure models, and angiotensin II-induced fibroblasts in vitro (Xu et al., 2022; Zhou et al., 2022). We also observed PS-NPs-induced upregulation of HIPK2 in our study. Whereas P53, Wnt/β-catenin, and TGF-β/Smad3 have been identified as classical downstream targets of HIPK2 (Jin et al., 2012).

The phosphorylation of P53 is an important pathway mediating apoptosis, and ser15 could cause cardiomyocyte apoptosis under ischemic conditions (Kim et al., 2013; Wang et al., 2013). Decreased P-P53 (ser15) facilitated the protective effect of storax against ISO-induced cardiomyocyte apoptosis (Xu et al., 2022). In our study, we found that PS-NPs increased the phosphorylation of P53, which might contribute to cardiac apoptosis. A recent scientific study reported that the phosphorylation of P53 was regulated by HIPK2 and that the inhibition of HIPK2 reduced its phosphorylation to protect against myocardial infarction (Zhou et al., 2021). Regarding PS-NPs-induced

cardiac apoptosis, we found that pharmacological inhibition of HIPK2 reduced apoptosis by decreasing P53 phosphorylation.

TGF-β1/Smad3 is a classical fibrosis-associated pathway involved in the progression of fibrosis in heart disease (Weng et al., 2023). Smad3 activation plays an important role in regulating cardiac fibrosis (Dobaczewski et al., 2010). In our study, we observed that PS-NPs activated the TGF-β1/Smad3 signaling pathway, causing elevated Smad3 phosphorylation, which might mediate the profibrotic effects of PS-NPs. Recently, a substantial amount of literature has revealed the protective role of HIPK2 in multiorgan fibrosis: inhibitors of HIPK2 attenuated renal fibrosis through inhibition of the TGF-β1/Smad3 pathway, knockdown of HIPK2 attenuated angiotensin-induced cardiac fibrosis through inhibition of the TGF-β1/Smad pathway, and phosphorylation of Smad3 was involved in the protection against heart failure mediated by HIPK2 inhibition (Liu et al., 2017; Xu et al., 2022; Zhou et al., 2022). Our findings revealed that PS-NPs upregulated Smad3 phosphorylation and TGF-β1, which were regulated by HIPK2, suggesting that HIPK2 inhibition mediated protection against cardiac fibrosis.

Our RNA sequencing results revealed that PS-NPs led to the upregulation of *Pdpr* and the activation of inflammation-associated pathways in both healthy and pathological state hearts. A recent study suggested that combined exposure to microplastics and Di (2-ethylhexyl) phthalate could exacerbate renal pyroptosis and inflammation in mice by activating the NF-κB/NLRP3 pathway (Li et al., 2024). However, our study focused primarily on *Hipk2*, demonstrating its significant role in PS-NPs-induced cardiotoxicity, particularly through its impact on cardiac apoptosis and fibrosis. Further in-depth studies are warranted to fully understand the broader implications of PS-NPs exposure, including other potentially involved mechanisms.

In addition, it must be acknowledged that this study has several other limitations. First, our research was limited to male mice, and future experiments should consider the inclusion of female mice to increase the generalizability of the findings on PS-NPs-induced cardiotoxicity. Second, although previous studies have reported the accumulation of PS-NPs in the mouse heart, the lack of quantification of PS-NPs in

cardiac tissue represents a potential limitation of the current study. Future experiments should aim to incorporate internal exposure assessments to better elucidate the mechanisms underlying the effects of environmental pollutants on cardiovascular health.

5. Conclusion

In conclusion, our study offers a comprehensive assessment of the cardiotoxic impacts of orally administered PS-NPs on both healthy and pathological heart conditions. We have shown that exposure to PS-NPs resulted in dose-dependent cardiotoxicity, predominantly characterized by enhanced apoptosis and fibrosis, rather than cardiac hypertrophy, particularly in pathological states. In addition, our findings highlighted the crucial role of HIPK2 in PS-NPs-related cardiotoxicity. This study enhances our understanding of the cardiac toxicological profile of PS-NPs and elucidates the underlying mechanisms involved, facilitating a more informed evaluation of the risks associated with PS-NPs exposure.

CRediT authorship contribution statement

Jian-Zheng Yang and Kai-Kai Zhang: Methodology, Investigation, Writing – Original Draft. **Clare Hsu and Lin Miao**: Resources, Software. **Li-Jian Chen and Jia-Li Liu**: Project administration, Software. **Jia-Hao Li and Xiu-Wen Li**: Resources. **Jia-Hao Zeng, Long Chen and Ji-Hui Li:** Validation, Formal analysis. **Xiao-Li Xie**: Conceptualization, Funding acquisition. **Qi Wang**: Funding acquisition, Supervision, Writing – Review & Editing.

Declaration of competing interest

The authors declare that they have no known competing financial interests or personal relationships that could have appeared to influence the work reported in this paper.

Acknowledgments

The graphical abstract was drawn by Figdraw (www.home-for-researchers.com). Flowcharts were created with BioRender.com.

Funding

This work was supported by the National Natural Science Foundation of China (Grant Nos. 82171877 and 82173474) and Guangdong Basic and Applied Basic Research Fo undation (Grant No. 2023A1515012476).

Data availability

The data used to support the findings of this study have been deposited in the NCBI Sequence Read Archive under accession no. PRJNA1070559.

References

Amato-Lourenço, L.F., Carvalho-Oliveira, R., Júnior, G.R., Dos, S.G.L., Ando, R.A., Mauad, T., 2021. Presence of airborne microplastics in human lung tissue. J. Hazard. Mater. 416126124. 10.1016/j.jhazmat.2021.126124.

Brunekreef, B., Hoffmann, B., 2016. Air pollution and heart disease. Lancet. 388 (10045), 640-642. 10.1016/S0140-6736(16)30375-0.

Bujak, M., Frangogiannis, N.G., 2007. The role of TGF-beta signaling in myocardial infarction and cardiac remodeling. Cardiovasc. Res. 74 (2), 184-195. 10.1016/j.cardiores.2006.10.002.

Conte, A., Pierantoni, G.M., 2018. Update on the Regulation of HIPK1, HIPK2 and HIPK3 Protein Kinases by microRNAs. Microrna. 7 (3), 178-186. 10.2174/2211536607666180525102330.

Deweerdt, S., 2022. How to make plastic less of an environmental burden. Nature. 611 (7936), S2-S5. 10.1038/d41586-022-03644-1.

Dobaczewski, M., Bujak, M., Li, N., Gonzalez-Quesada, C., Mendoza, L.H., Wang, X.F., Frangogiannis, N.G., 2010. Smad3 signaling critically regulates fibroblast phenotype and function in healing myocardial infarction. Circ. Res. 107 (3), 418-428. 10.1161/CIRCRESAHA.109.216101.

Fournier, S.B., D'Errico, J.N., Adler, D.S., Kollontzi, S., Goedken, M.J., Fabris, L., Yurkow, E.J., Stapleton, P.A., 2020. Nanopolystyrene translocation and fetal deposition after acute lung exposure during late-stage pregnancy. Part. Fibre Toxicol. 17 (1), 55. 10.1186/s12989-020-00385-9.

Guo, Y., Sui, J.Y., Kim, K., Zhang, Z., Qu, X.A., Nam, Y.J., Willette, R.N., Barnett, J.V., Knollmann,

B.C., Force, T., Lal, H., 2019. Cardiomyocyte Homeodomain-Interacting Protein Kinase 2 Maintains Basal Cardiac Function via Extracellular Signal-Regulated Kinase Signaling. Circulation. 140 (22), 1820-1833. 10.1161/CIRCULATIONAHA.119.040740.

Guo, Z., Hu, Y.H., Feng, G.S., Valenzuela, R.C., Li, Z.Z., Cai, S.D., Wang, Q.Q., Luo, W.W., Li, Q., Liang, L.Y., Wu, Z.K., Zhang, J.G., Javaheri, A., Wang, L., Lu, J., Liu, P.Q., 2023. JMJD6 protects against isoproterenol-induced cardiac hypertrophy via inhibition of NF-κB activation by demethylating R149 of the p65 subunit. Acta Pharmacol. Sin. 44 (9), 1777-1789. 10.1038/s41401-023-01086-7.

He, P., Yu, Z.J., Sun, C.Y., Jiao, S.J., Jiang, H.Q., 2017. Knockdown of HIPK2 attenuates the pro-fibrogenic response of hepatic stellate cells induced by TGF-β1. Biomed. Pharmacother. 85575-581. 10.1016/j.biopha.2016.11.066.

Huang, J., Sun, X., Wang, Y., Su, J., Li, G., Wang, X., Yang, Y., Zhang, Y., Li, B., Zhang, G., Li, J., Du J, Nanjundappa, R.H., Umeshappa, C.S., Shao, K., 2023. Biological interactions of polystyrene nanoplastics: Their cytotoxic and immunotoxic effects on the hepatic and enteric systems. Ecotoxicol. Environ. Saf. 264115447. 10.1016/j.ecoenv.2023.115447.

Ishiura, J., Nakamori, S., Ishida, M., Dohi, K., 2022. 'Targeting the cardiac myocyte and fibrosis' in heart failure. Eur. Heart J. 43 (5), 432. 10.1093/eurheartj/ehab780.

Jin, Y., Ratnam, K., Chuang, P.Y., Fan, Y., Zhong, Y., Dai, Y., Mazloom, A.R., Chen, E.Y., D'Agati, V., Xiong, H., Ross, M.J., Chen, N., Ma'Ayan, A., He, J.C., 2012. A systems approach identifies HIPK2 as a key regulator of kidney fibrosis. Nat. Med. 18 (4), 580-588. 10.1038/nm.2685.

Jing, J., Zhang, L., Han, L., Wang, J., Zhang, W., Liu, Z., Gao, A., 2022. Polystyrene micro-/nanoplastics induced hematopoietic damages via the crosstalk of gut microbiota, metabolites, and cytokines. Environ. Int. 161107131. 10.1016/j.envint.2022.107131.

Kang, H., Zhang, W., Jing, J., Huang, D., Zhang, L., Wang, J., Han, L., Liu, Z., Wang, Z., Gao, A., 2023. The gut-brain axis involved in polystyrene nanoplastics-induced neurotoxicity via reprogramming the circadian rhythm-related pathways. J. Hazard. Mater. 458131949. 10.1016/j.jhazmat.2023.131949.

Kim, Y.A., Kim, M.Y., Yu, H.Y., Mishra, S.K., Lee, J.H., Choi, K.S., Kim, J.H., Xiang, Y.K., Jung, Y.S., 2013. Gadd45β is transcriptionally activated by p53 via p38α-mediated phosphorylation during myocardial ischemic injury. J. Mol. Med. 91 (11), 1303-1313. 10.1007/s00109-013-1070-9.

Kim, Y.H., Choi, C.Y., Lee, S.J., Conti, M.A., Kim, Y., 1998. Homeodomain-interacting protein kinases, a novel family of co-repressors for homeodomain transcription factors. J. Biol. Chem. 273 (40), 25875-25879. 10.1074/jbc.273.40.25875.

Li, S., Gu, X., Zhang, M., Jiang, Q., Xu, T., 2024. Di (2-ethylhexyl) phthalate and polystyrene microplastics co-exposure caused oxidative stress to activate NF-κB/NLRP3 pathway aggravated pyroptosis and inflammation in mouse kidney. Sci. Total Environ. 926171817. 10.1016/j.scitotenv.2024.171817.

Li, Y., Ye, Y., Rihan, N., Jiang, Q., Liu, X., Zhao, Y., Che, X., 2023. Polystyrene nanoplastics decrease nutrient accumulation, disturb sex hormones, and inhibit reproductive development in juvenile Macrobrachium nipponense. Sci. Total Environ. 891164481. 10.1016/j.scitotenv.2023.164481.

Liang, B., Huang, Y., Zhong, Y., Li, Z., Ye, R., Wang, B., Zhang, B., Meng, H., Lin, X., Du J, Hu, M., Wu, Q., Sui, H., Yang, X., Huang, Z., 2022. Brain single-nucleus transcriptomics highlights that polystyrene nanoplastics potentially induce Parkinson's disease-like neurodegeneration by causing energy metabolism disorders in mice. J. Hazard. Mater. 430128459. 10.1016/j.jhazmat.2022.128459.

Liang, B., Zhong, Y., Huang, Y., Lin, X., Liu, J., Lin, L., Hu, M., Jiang, J., Dai, M., Wang, B., Zhang, B., Meng, H., Lelaka, J., Sui, H., Yang, X., Huang, Z., 2021. Underestimated health risks: polystyrene micro- and nanoplastics jointly induce intestinal barrier dysfunction by ROS-mediated epithelial cell apoptosis. Part. Fibre Toxicol. 18 (1), 20. 10.1186/s12989-021-00414-1.

Lim, X., 2021. Microplastics are everywhere - but are they harmful? Nature. 593 (7857), 22-25. 10.1038/d41586-021-01143-3.

Lin, H., Zhang, J., Ni, T., Lin, N., Meng, L., Gao, F., Luo, H., Liu, X., Chi, J., Guo, H., 2019. Yellow Wine Polyphenolic Compounds prevents Doxorubicin-induced cardiotoxicity through activation of the Nrf2 signalling pathway. J. Cell. Mol. Med. 23 (9), 6034-6047. 10.1111/jcmm.14466.

Lin, P., Tong, X., Xue, F., Qianru, C., Xinyu, T., Zhe, L., Zhikun, B., Shu, L., 2022. Polystyrene nanoplastics exacerbate lipopolysaccharide-induced myocardial fibrosis and autophagy in mice via ROS/TGF-β1/Smad. Toxicology. 480153338. 10.1016/j.tox.2022.153338.

Liu, R., Das, B., Xiao, W., Li, Z., Li, H., Lee, K., He, J.C., 2017. A Novel Inhibitor of Homeodomain Interacting Protein Kinase 2 Mitigates Kidney Fibrosis through Inhibition of the TGF-β1/Smad3 Pathway. J. Am. Soc. Nephrol. 28 (7), 2133-2143. 10.1681/ASN.2016080841.

Luo, H., Liu, C., He, D., Sun, J., Li, J., Pan, X., 2022. Effects of aging on environmental behavior of plastic additives: Migration, leaching, and ecotoxicity. Sci. Total Environ. 849157951. 10.1016/j.scitotenv.2022.157951.

Ma, J., Wan, Y., Song, L., Wang, L., Wang, H., Li, Y., Huang, D., 2023. Polystyrene nanobeads exacerbate chronic colitis in mice involving in oxidative stress and hepatic lipid metabolism. Part. Fibre Toxicol. 20 (1), 49. 10.1186/s12989-023-00560-8.

Manzano-Covarrubias, A.L., Yan, H., Luu, M., Gadjdjoe, P.S., Dolga, A.M., Schmidt, M., 2023. Unravelling the signaling power of pollutants. Trends Pharmacol. Sci. 44 (12), 917-933. 10.1016/j.tips.2023.09.002.

Nair, A.B., Jacob, S., 2016. A simple practice guide for dose conversion between animals and human. J Basic Clin Pharm. 7 (2), 27-31. 10.4103/0976-0105.177703.

Prata, J.C., Da, C.J., Lopes, I., Duarte, A.C., Rocha-Santos, T., 2020. Environmental exposure to microplastics: An overview on possible human health effects. Sci. Total Environ. 702134455. 10.1016/j.scitotenv.2019.134455.

Ragusa, A., Svelato, A., Santacroce, C., Catalano, P., Notarstefano, V., Carnevali, O., Papa, F., Rongioletti, M., Baiocco, F., Draghi, S., D'Amore, E., Rinaldo, D., Matta, M., Giorgini, E., 2021. Plasticenta: First evidence of microplastics in human placenta. Environ. Int. 146106274. 10.1016/j.envint.2020.106274.

Rai, P.K., Lee, J., Brown, R., Kim, K.H., 2021. Environmental fate, ecotoxicity biomarkers, and potential health effects of micro- and nano-scale plastic contamination. J. Hazard. Mater. 403123910. 10.1016/j.jhazmat.2020.123910.

Rajagopalan, S., Landrigan, P.J., 2021. Pollution and the Heart. N. Engl. J. Med. 385 (20), 1881-1892. 10.1056/NEJMra2030281.

Ritter, O., Schmitz, M.L., 2019. Differential intracellular localization and dynamic nucleocytoplasmic shuttling of homeodomain-interacting protein kinase family members. Biochim. Biophys. Acta-Mol. Cell Res. 1866 (10), 1676-1686. 10.1016/j.bbamcr.2019.04.009.

Senathirajah, K., Attwood, S., Bhagwat, G., Carbery, M., Wilson, S., Palanisami, T., 2021. Estimation of the mass of microplastics ingested - A pivotal first step towards human health risk assessment. J. Hazard. Mater. 404 (Pt B), 124004. 10.1016/j.jhazmat.2020.124004.

Sun, X.D., Yuan, X.Z., Jia, Y., Feng, L.J., Zhu, F.P., Dong, S.S., Liu, J., Kong, X., Tian, H., Duan, J.L., Ding, Z., Wang, S.G., Xing, B., 2020. Differentially charged nanoplastics demonstrate distinct accumulation in Arabidopsis thaliana. Nat. Nanotechnol. 15 (9), 755-760. 10.1038/s41565-020-0707-4.

Tang, Y., Zhao, R., Pu, Q., Jiang, S., Yu, F., Yang, Z., Han, T., 2023. Investigation of nephrotoxicity on mice exposed to polystyrene nanoplastics and the potential amelioration effects of DHA-enriched phosphatidylserine. Sci. Total Environ. 892164808. 10.1016/j.scitotenv.2023.164808.

Wagner, S., Reemtsma, T., 2019. Things we know and don't know about nanoplastic in the environment. Nat. Nanotechnol. 14 (4), 300-301. 10.1038/s41565-019-0424-z.

Wang, B., Li, D., Kovalchuk, O., 2013. p53 Ser15 phosphorylation and histone modifications contribute to IR-induced miR-34a transcription in mammary epithelial cells. Cell Cycle. 12 (13), 2073-2083. 10.4161/cc.25135.

Wang, B., Liang, B., Huang, Y., Li, Z., Zhang, B., Du J, Ye, R., Xian, H., Deng, Y., Xiu, J., Yang, X., Ichihara, S., Ichihara, G., Zhong, Y., Huang, Z., 2023. Long-Chain Acyl Carnitines Aggravate Polystyrene Nanoplastics-Induced Atherosclerosis by Upregulating MARCO. Adv. Sci. 10 (19), e2205876. 10.1002/advs.202205876.

Wang, M., Qian, L., Li, J., Ming, H., Fang, L., Li, Y., Zhang, M., Xu, Y., Ban, Y., Zhang, W., Zhang, Y., Liu, Y., Wang, N., 2020. GHSR deficiency exacerbates cardiac fibrosis: role in macrophage inflammasome activation and myofibroblast differentiation. Cardiovasc. Res. 116 (13), 2091-2102. 10.1093/cvr/cvz318.

Wang, M., Zhou, T., Song, Y., Li, X., Ma, H., Hu, Y., Heianza, Y., Qi, L., 2021. Joint exposure to various ambient air pollutants and incident heart failure: a prospective analysis in UK Biobank. Eur. Heart J. 42 (16), 1582-1591. 10.1093/eurheartj/ehaa1031.

Wang, P., Xu, S., Xu, J., Xin, Y., Lu, Y., Zhang, H., Zhou, B., Xu, H., Sheu, S.S., Tian, R., Wang, W., 2022. Elevated MCU Expression by CaMKIIδB Limits Pathological Cardiac Remodeling. Circulation. 145 (14), 1067-1083. 10.1161/CIRCULATIONAHA.121.055841.

Wang, W., Mao, X., Zhang, R., Zhou, X.X., Liu, Y., Zhou, H., Jia, J., Yan, B., 2023. Nanoplastic Exposure at Environmental Concentrations Disrupts Hepatic Lipid Metabolism through Oxidative Stress Induction and Endoplasmic Reticulum Homeostasis Perturbation. Environ. Sci. Technol. 57 (38), 14127-14137. 10.1021/acs.est.3c02769.

Weng, L., Ye, J., Yang, F., Jia, S., Leng, M., Jia, B., Xu, C., Zhao, Y., Liu, R., Xiong, Y., Zhou, Y., Zhao, J., Zheng, M., 2023. TGF-β1/SMAD3 Regulates Programmed Cell Death 5 That Suppresses Cardiac Fibrosis Post-Myocardial Infarction by Inhibiting HDAC3. Circ. Res. 133 (3), 237-251. 10.1161/CIRCRESAHA.123.322596.

Wu, H., Eckhardt, C.M., Baccarelli, A.A., 2023. Molecular mechanisms of environmental exposures and human disease. Nat. Rev. Genet. 24 (5), 332-344. 10.1038/s41576-022-00569-3.

Xu, D., Ma, Y., Peng, C., Gan, Y., Wang, Y., Chen, Z., Han, X., Chen, Y., 2023. Differently surface-labeled polystyrene nanoplastics at an environmentally relevant concentration induced Crohn's ileitis-like features via triggering intestinal epithelial cell necroptosis. Environ. Int. 176107968. 10.1016/j.envint.2023.107968.

Xu, F., Mao, B., Li, Y., Zhao, Y., 2022. Knockdown of HIPK2 Attenuates Angiotensin II-Induced Cardiac Fibrosis in Cardiac Fibroblasts. J. Cardiovasc. Pharmacol. 80 (1), 125-131. 10.1097/FJC.0000000000001292.

Xu, Z., Lu, D., Yuan, J., Wang, L., Wang, J., Lei, Z., Liu, S., Wu, J., Wang, J., Huang, L., 2022. Storax

Attenuates Cardiac Fibrosis following Acute Myocardial Infarction in Rats via Suppression of AT1R-Ankrd1-P53 Signaling Pathway. Int. J. Mol. Sci. 23 (21). 10.3390/ijms232113161.

Yang, J.Z., Zhang, K.K., He, J.T., Chen, L.J., Ding, J.F., Liu, J.L., Li, J.H., Liu, Y., Li, X.W., Zhao, D., Xie, X.L., Wang, Q., 2023. Obeticholic acid protects against methamphetamine-induced anxiety-like behavior by ameliorating microbiota-mediated intestinal barrier impairment. Toxicology. 486153447. 10.1016/j.tox.2023.153447.

Yang, J.Z., Zhang, K.K., Liu, Y., Li, X.W., Chen, L.J., Liu, J.L., Li, J.H., Chen, L., Hsu, C., Zeng, J.H., Xie, X.L., Wang, Q., 2023. Epigallocatechin-3-gallate ameliorates polystyrene microplastics-induced anxiety-like behavior in mice by modulating gut microbe homeostasis. Sci. Total Environ. 892164619. 10.1016/j.scitotenv.2023.164619.

Yang, J.Z., Zhang, K.K., Shen, H.W., Liu, Y., Li, X.W., Chen, L.J., Liu, J.L., Li, J.H., Zhao, D., Wang, Q., Zhou, C.S., 2023. Sigma-1 receptor knockout disturbs gut microbiota, remodels serum metabolome, and exacerbates isoprenaline-induced heart failure. Front. Microbiol. 141255971. 10.3389/fmicb.2023.1255971.

Zha, H., Xia, J., Wang, K., Xu, L., Chang, K., Li, L., 2023. Foodborne and airborne polyethersulfone nanoplastics respectively induce liver and lung injury in mice: Comparison with microplastics. Environ. Int. 183108350. 10.1016/j.envint.2023.108350.

Zhang, K., Chen, L., Yang, J., Liu, J., Li, J., Liu, Y., Li, X., Chen, L., Hsu, C., Zeng, J., Xie, X., Wang, Q., 2023. Gut microbiota-derived short-chain fatty acids ameliorate methamphetamine-induced depression- and anxiety-like behaviors in a Sigmar-1 receptor-dependent manner. Acta Pharm. Sin. B. 13 (12), 4801-4822. 10.1016/j.apsb.2023.09.010.

Zhang, K., Yang, J., Chen, L., He, J., Qu, D., Zhang, Z., Liu, Y., Li, X., Liu, J., Li, J., Xie, X., Wang, Q., 2023. Gut Microbiota Participates in Polystyrene Microplastics-Induced Hepatic Injuries by Modulating the Gut-Liver Axis. ACS Nano. 17 (15), 15125-15145. 10.1021/acsnano.3c04449.

Zhang, K.K., Chen, L.J., Li, J.H., Liu, J.L., Wang, L.B., Xu, L.L., Yang, J.Z., Li, X.W., Xie, X.L., Wang, Q., 2022. Methamphetamine Disturbs Gut Homeostasis and Reshapes Serum Metabolome, Inducing Neurotoxicity and Abnormal Behaviors in Mice. Front. Microbiol. 13755189. 10.3389/fmicb.2022.755189.

Zhang, Y., Ding, Y., Li, M., Yuan, J., Yu, Y., Bi, X., Hong, H., Ye, J., Liu, P., 2022. MicroRNA-34c-5p provokes isoprenaline-induced cardiac hypertrophy by modulating autophagy via targeting ATG4B. Acta Pharm. Sin. B. 12 (5), 2374-2390. 10.1016/j.apsb.2021.09.020.

Zhang, Y., Yin, K., Wang, D., Wang, Y., Lu, H., Zhao, H., Xing, M., 2022. Polystyrene microplastics-induced cardiotoxicity in chickens via the ROS-driven NF-κB-NLRP3-GSDMD and AMPK-PGC-1α axes. Sci. Total Environ. 840156727. 10.1016/j.scitotenv.2022.156727.

Zhou, Q., Deng, J., Yao, J., Song, J., Meng, D., Zhu, Y., Xu, M., Liang, Y., Xu, J., Sluijter, J.P., Xiao, J., 2021. Exercise downregulates HIPK2 and HIPK2 inhibition protects against myocardial infarction. EBioMedicine. 74103713. 10.1016/j.ebiom.2021.103713.

Zhou, Q., Meng, D., Li, F., Zhang, X., Liu, L., Zhu, Y., Liu, S., Xu, M., Deng, J., Lei, Z., Sluijter, J., Xiao, J., 2022. Inhibition of HIPK2 protects stress-induced pathological cardiac remodeling. EBioMedicine. 85104274. 10.1016/j.ebiom.2022.104274.

Zhou, Y., Wu, Q., Li, Y., Feng, Y., Wang, Y., Cheng, W., 2023. Low-dose of polystyrene microplastics induce cardiotoxicity in mice and human-originated cardiac organoids. Environ. Int. 179108171. 10.1016/j.envint.2023.108171.

Figure captions

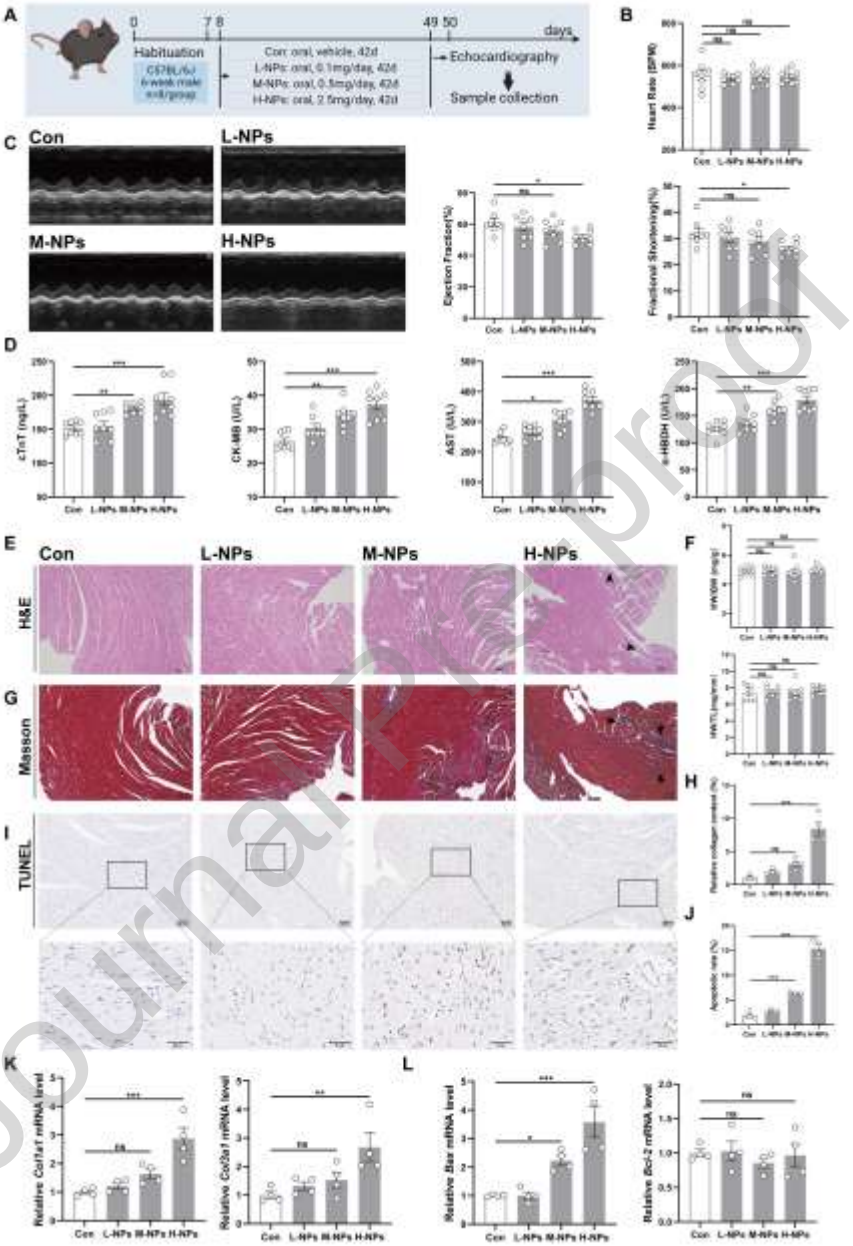

Figure 1. Dose-dependent induction of cardiotoxicity by oral PS-NPs. (A) Flowchart of Experiment I. (B) Effect of PS-NPs on heart rate in mice. (C) Representative M-mode echocardiograms and measurements of EF and FS. (D) PS-NPs increased the serum levels of markers of myocardial injury. (E) Representative H&E-stained heart sections (scale bars, 100 μm). (F) HW/BW and HW/TL were calculated for each group. (G-H) Representative Masson-stained cardiac sections and their quantification (scale bars, 100

μm) (black arrows represented collagen fiber deposition). (I-J) Representative TUNEL-stained cardiac sections and their quantification (scale bars, 100 μm and 50 μm). (K-L) Relative expression of the heart fibrosis- and apoptosis-related mRNAs *Col1a1*, *Col3a1*, *Bax*, and *Bcl-2* across the groups. The data were presented as mean ± SEM. n=4-8 per group. Significant differences were determined by one-way ANOVA with Tukey's multiple comparisons test or the Kruskal–Wallis test followed by Dunn's post hoc test. *: $p<0.05$, **: $p<0.01$, ***: $p<0.001$ versus respective control.

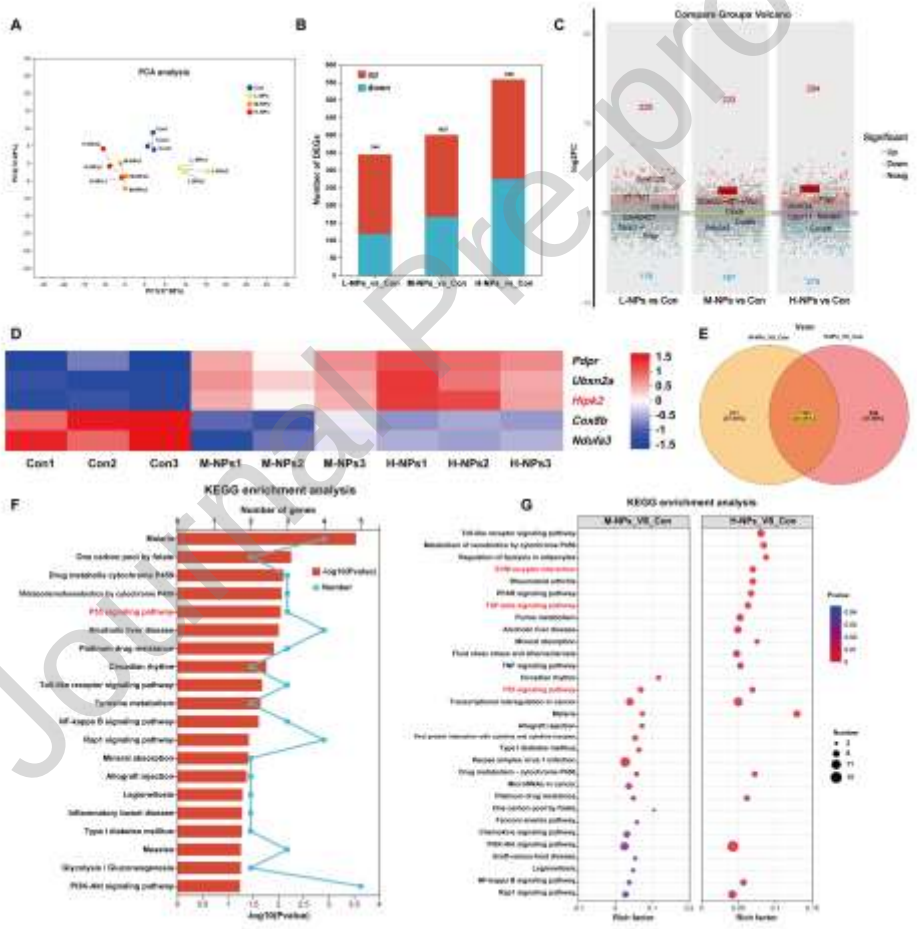

Figure 2. RNA sequencing of the Con, L-NPs, M-NPs and H-NPs groups. (A) PCA of the four groups. (B) The number of DEGs induced by PS-NPs was dose dependent compared to the Con group. (C) Compare groups volcano screened for 6 genes with the most significant p value. (D) Clustering heatmap of five genes co-regulated by M-NPs and H-NPs. (E) Venn diagram analysis of the Con, M-NPs and H-NPs groups. (F)

KEGG enrichment analysis of 189 DEGs. (G) Additional enrichment of DEGs between the H-NPs and Con groups to fibrosis-related pathways. n=3 per group.

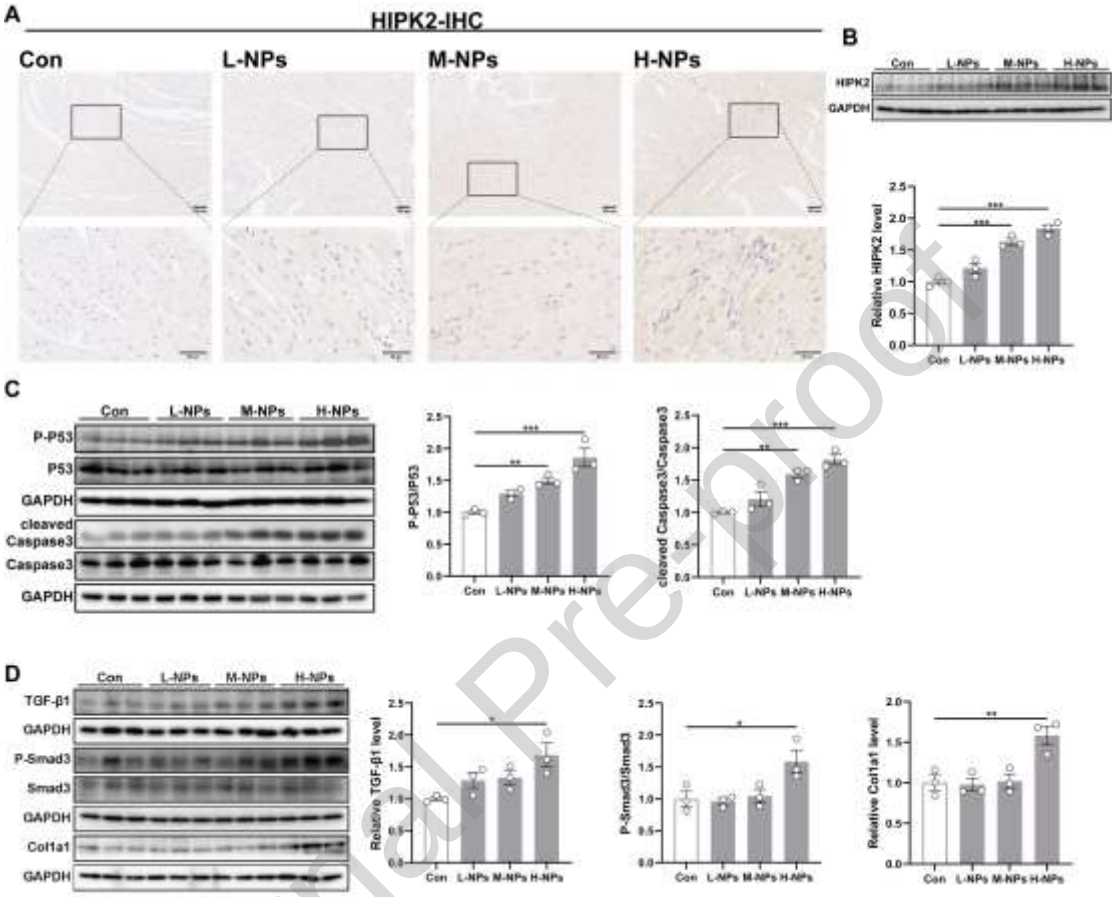

Figure 3. PS-NPs upregulated HIPK2, promoted P53 phosphorylation, and activated the TGF-β1/Smad3 pathway. (A) HIPK2 expression in IHC-stained heart sections (scale bars, 100 μm and 50 μm). (B) WB analysis validated the upregulation of HIPK2 in cardiac tissue. (C) The expression of proteins P-P53, P53, cleaved Caspase3, and Caspase3 in the heart. (D) WB analysis of the expression of proteins TGF-β1, P-Smad3, Smad3, and Col1a1 among the groups. The data were presented as mean ± SEM. n=3 per group. Significant differences were determined by one-way ANOVA with Tukey's multiple comparisons test. *: $p<0.05$, **: $p<0.01$, ***: $p<0.001$ versus respective control.

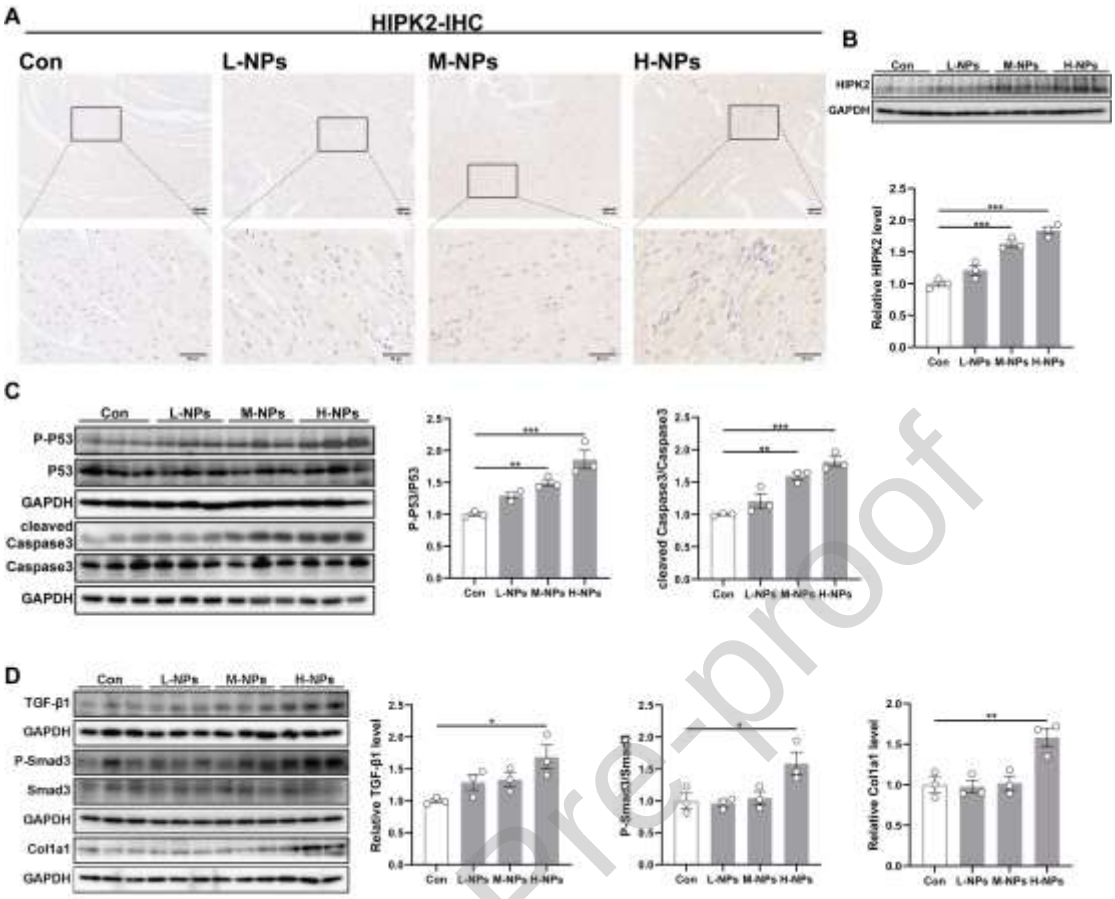

Figure 4. PS-NPs exacerbated ISO-induced cardiac remodeling. (A) Flowchart of Experiment II; (B) Heart rate monitoring for TTE analysis. (C) Representative echocardiograms and measurements of EF and FS. (D) Serum levels of the myocardial injury markers cTnT, CK-MB, AST and α-HBDH. (E) Representative H&E-stained heart sections (scale bars, 100 μm). (F) HW/BW and HW/TL were calculated for each group. (G-H) Representative plots and quantification of ISO-induced cardiac fibrosis exacerbated by M-NPs (scale bars, 100 μm) (black arrows represented collagen fiber deposition). (I-J) Representative TUNEL-stained cardiac sections and their quantification (scale bars, 100 μm and 50 μm). (K-L) The mRNA levels of *Col1a1*, *Col3a1*, *Bax* and *Bcl-2*. The data were presented as mean ± SEM. n=4-8 per group. Significant differences were determined by two-way ANOVA with Tukey's multiple comparisons test or the Kruskal–Wallis test followed by Dunn's post hoc test. *: $p<0.05$, **: $p<0.01$, ***: $p<0.001$ versus respective control.

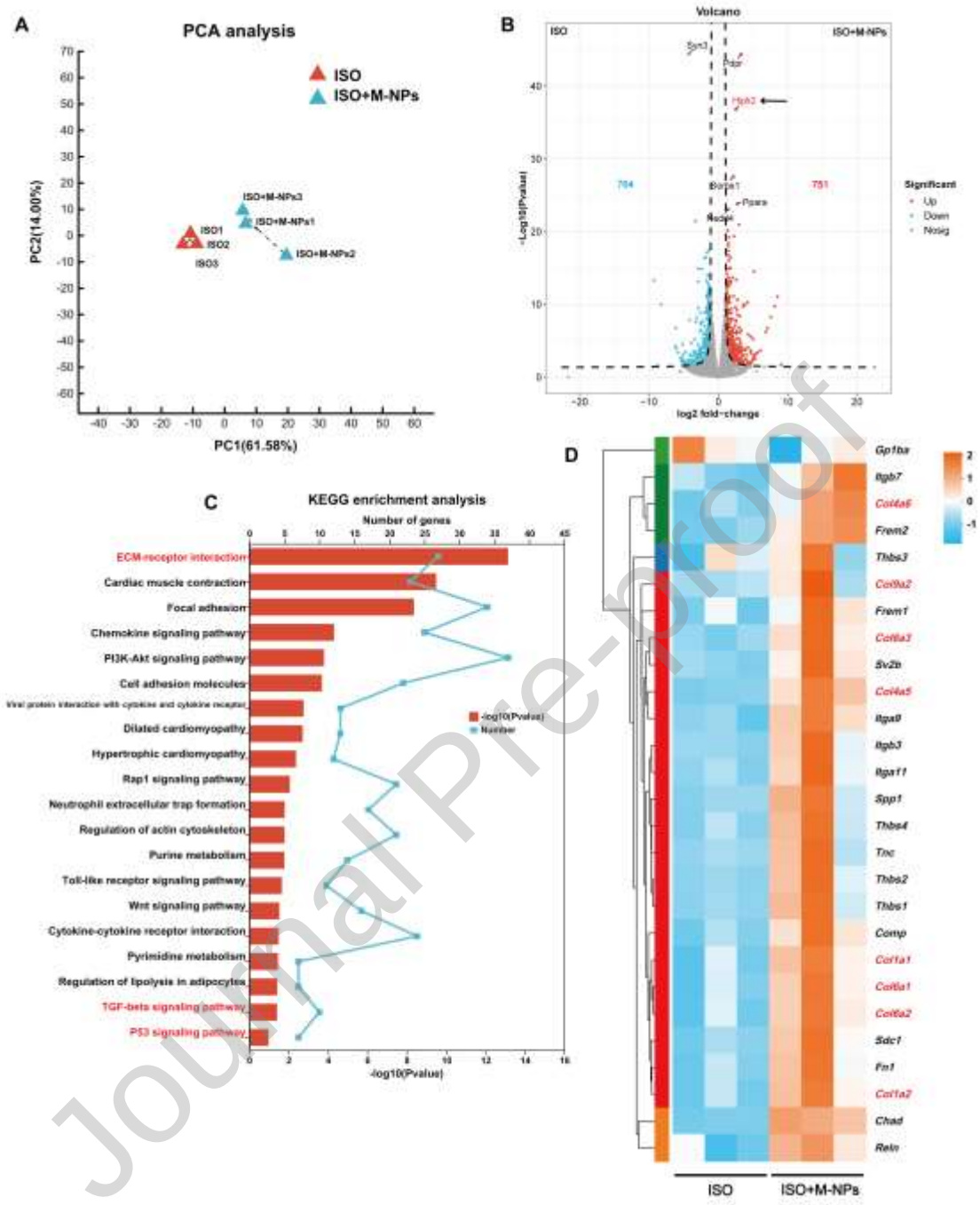

Figure 5. RNA sequencing analysis of the ISO and ISO+M-NPs groups. (A) PCA showed that the two groups clustered separately. (B) Volcano plot of DEGs between the two groups. (C) KEGG enrichment analysis of 1515 DEGs. (D) Heatmap showed numerous up-regulated fibrosis-related genes. n=3 per group.

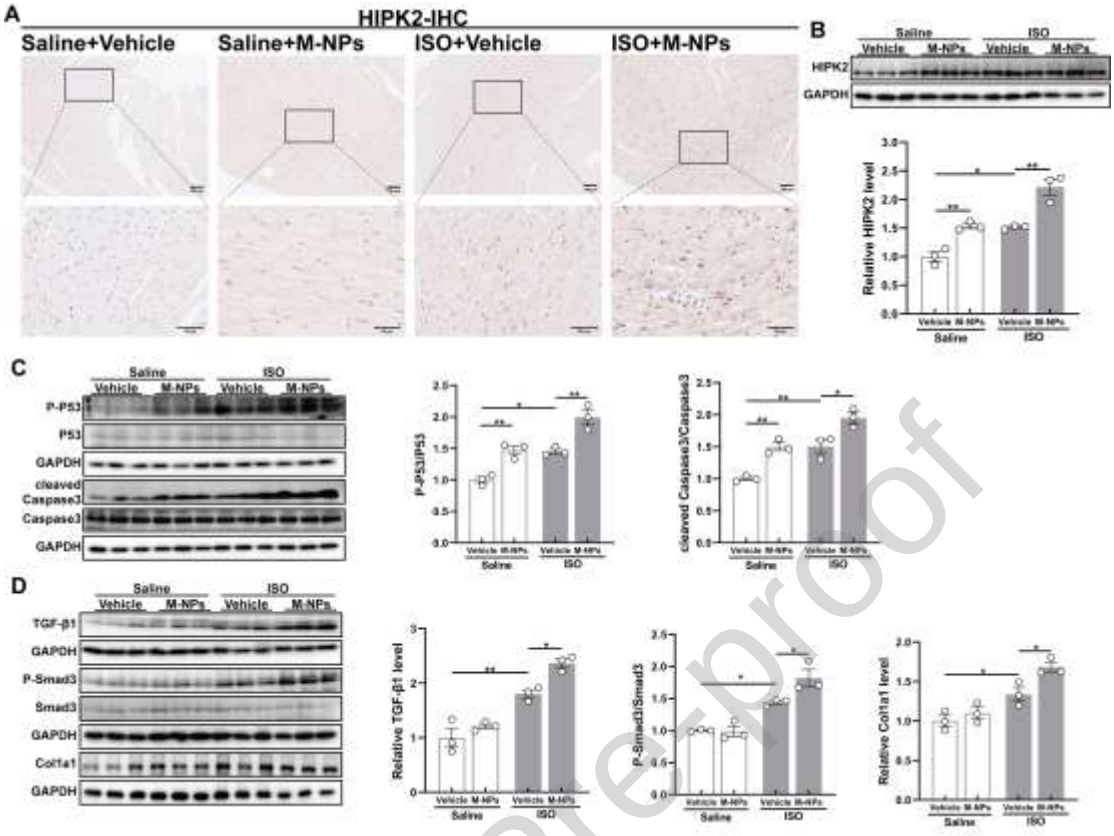

Figure 6. M-NPs further increased ISO-induced P53 phosphorylation and TGF-β1/Smad3 pathway activation. (A) HIPK2 expression in IHC-stained heart sections (scale bars, 100 μm and 50 μm). (B) PS-NPs promoted the protein expression of HIPK2. (C) The protein expression of P-P53, P53, cleaved Caspase3, and Caspase3 in the heart. (D) WB analysis of the protein expression of TGF-β1, P-Smad3, Smad3, and Col1a1 among the four groups. The data were presented as mean ± SEM. n=3 per group. Significant differences were determined by two-way ANOVA with Tukey's multiple comparisons test. *: $p<0.05$, **: $p<0.01$ versus respective control.

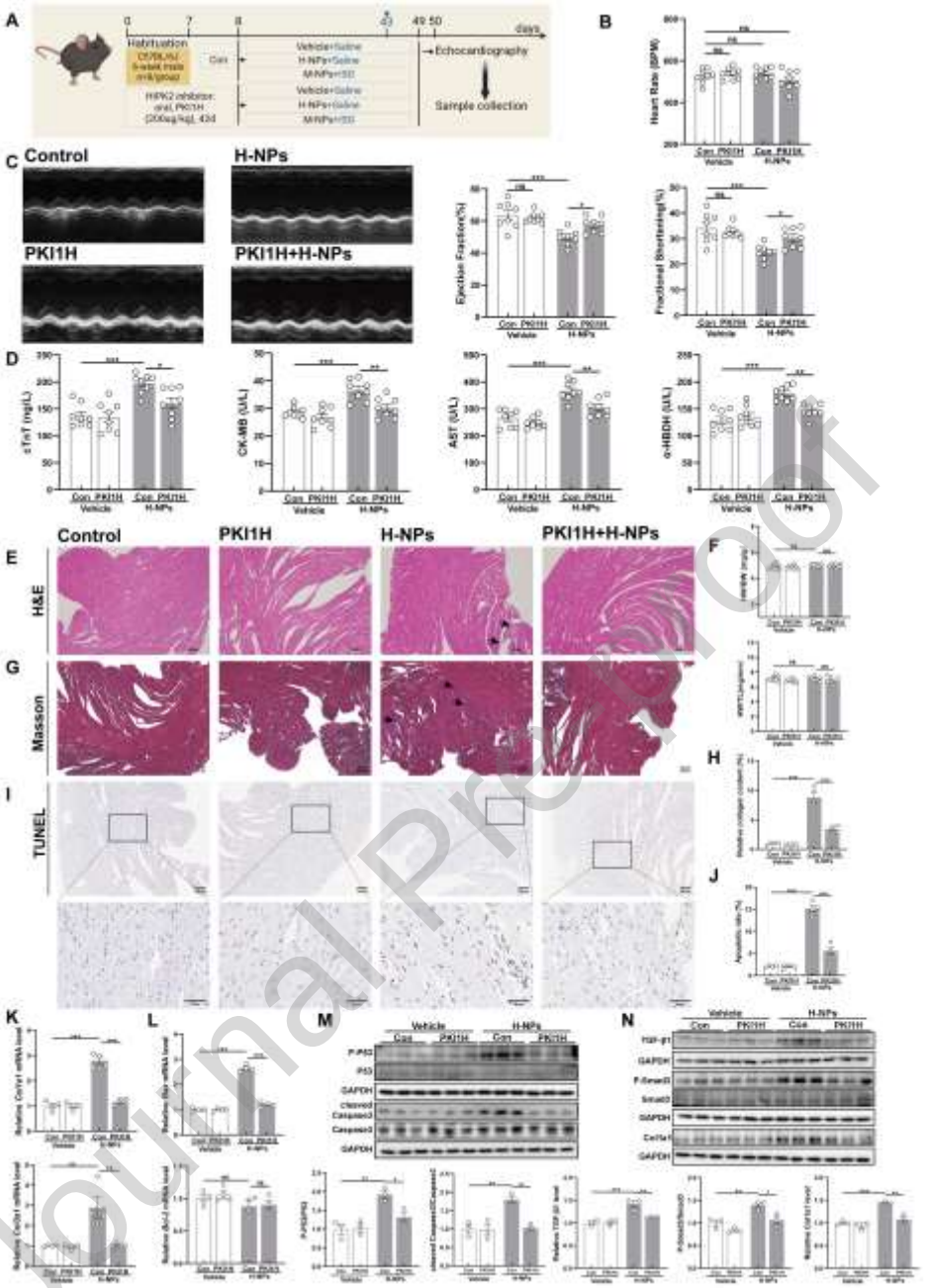

Figure 7. HIPK2 inhibition protected against H-NPs-induced cardiotoxicity. (A) Flowchart of Experiment III. (B-C) PKI1H ameliorated the H-NPs-induced decreases in EF and FS. (D) The concentrations of serum cTnT, CK-MB, AST and α-HBDH across the four groups. (E) Representative images of H&E-stained heart sections (scale bars, 100 μm). (F) HW/BW and HW/TL were calculated for each group. (G-H) Representative Masson-stained cardiac sections and quantification (scale bars, 100 μm) (black arrows represented collagen fiber deposition). (I-J) Representative TUNEL-stained cardiac sections and quantification (scale bars, 100 μm and 50 μm). (K-L)

Relative expression of *Col1a1*, *Col3a1*, *Bax* and *Bcl-2* at the mRNA level, normalized by mRNA GAPDH. (M) WB analysis of the P-P53/P53 and cleaved Caspase3/Caspase3 ratios. (N) The protein expression of TGF-β1, P-Smad3, Smad3 and Col1a1 in the heart. The data were presented as mean ± SEM. n=3-8 per group. Significant differences were determined by two-way ANOVA with Tukey's multiple comparisons test. *: p<0.05, **: p<0.01, ***: p<0.001 versus respective control.

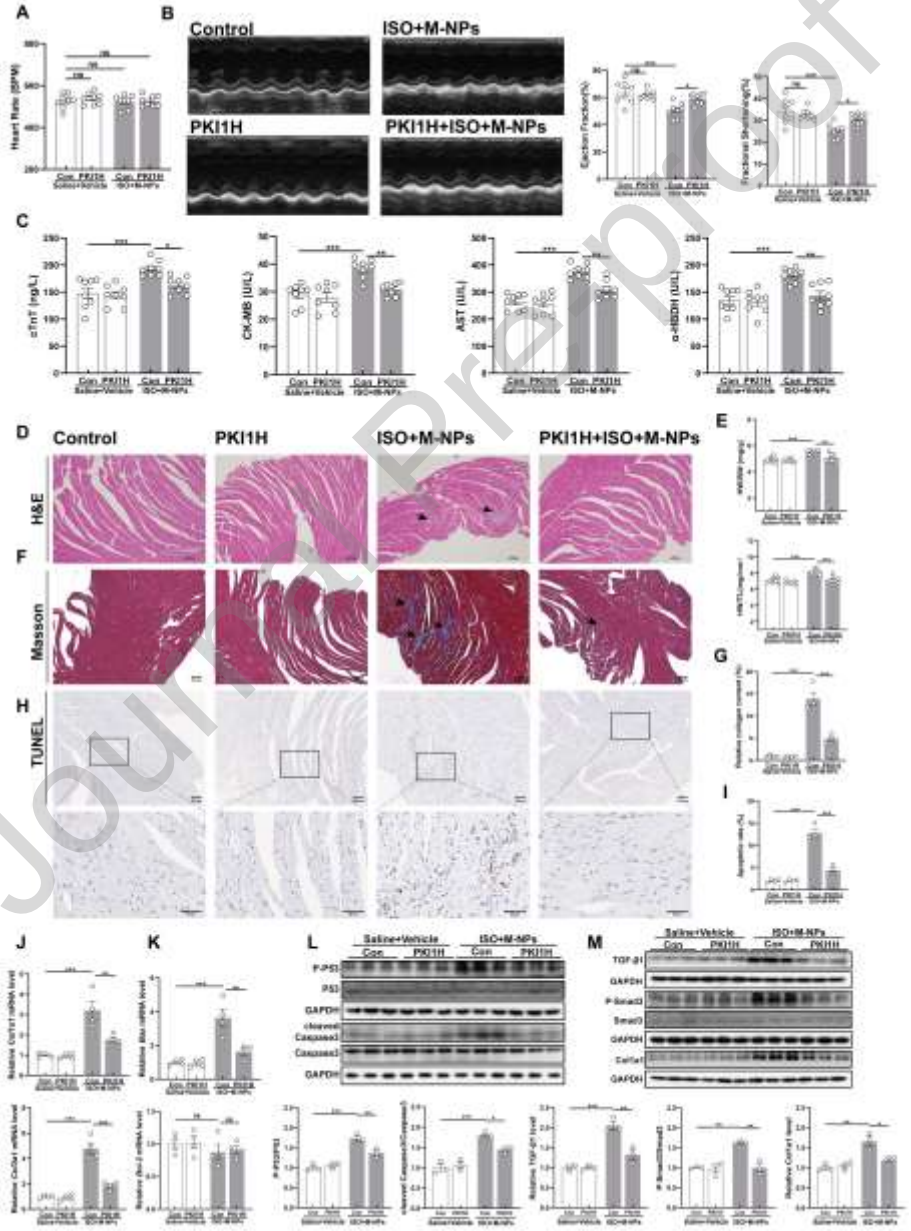

Figure 8. PKI1H protects against ISO+M-NPs-induced cardiotoxicity. (A-B) PKI1H ameliorated the ISO+M-NPs-induced decreases in EF and FS. (C) The concentrations of serum cTnT, CK-MB, AST and α-HBDH among the four groups. (D) Representative

images of H&E-stained heart sections (scale bars, 100 μm). (E) PKI1H reversed ISO+M-NPs-induced cardiac hypertrophy. (F-G) Representative Masson-stained cardiac sections and quantification (scale bars, 100 μm) (black arrows represented collagen fiber deposition). (H-I) Images and quantification of TUNEL-stained representative heart sections (scale bars, 100 μm and 50 μm). (J-K) Relative expression of *Col1a1*, *Col3a1*, *Bax* and *Bcl-2* at the mRNA level, normalized by mRNA GAPDH. (L) WB analysis of the P-P53/P53 and cleaved Caspase3/Caspase3 ratios among the four groups. (M) The protein expression of TGF-β1, P-Smad3, Smad3 and Col1a1 in the heart. The data were presented as mean ± SEM. n=3-8 per group. Significant differences were determined by two-way ANOVA with Tukey's multiple comparisons test. *: $p<0.05$, **: $p<0.01$, ***: $p<0.001$ versus respective control.

Graphical abstract

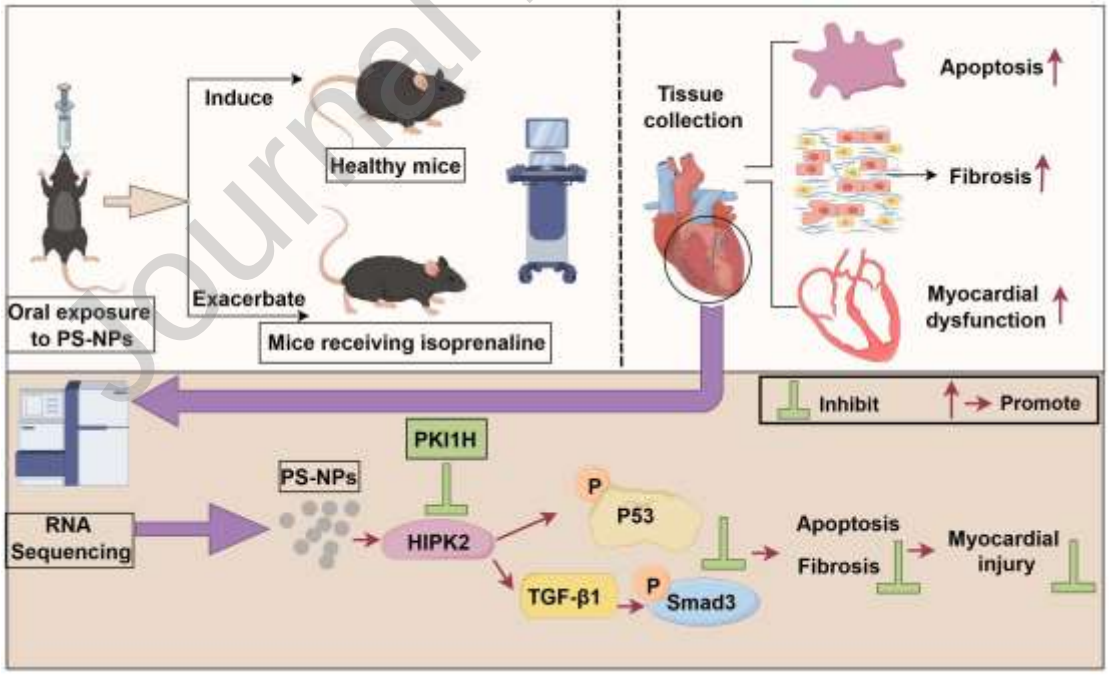

Declaration of interests

☒ The authors declare that they have no known competing financial interests or personal relationships that could have appeared to influence the work reported in this paper.

Highlights

- Exposure to PS-NPs induces cardiotoxicity in a dose-dependent manner.
- PS-NPs exacerbate cardiac apoptosis and fibrosis in pathological states.
- PS-NPs upregulate HIPK2 and activate the P53 and TGF-β1/Smad3 pathways.
- Inhibition of HIPK2 contributes to protection against PS-NPs-induced cardiotoxicity.